Investigation of Open Air Stability of CsPbBr$_3$ Thin-Film Growth on Different Substrates

Nicola Calisi and **Stefano Caporali** *

Department of Industrial Engineering, University of Florence, Via di Santa Marta 3, 50139 Firenze (FI), Italy; nicola.calisi@unifi.it

* Correspondence: stefano.caporali@unifi.it

check for updates

Abstract: Originally developed out of scientific curiosity, lead halide perovskites are rapidly gaining success due to their broad tenability and ease of fabrication. Despite these advantages and the considerable progress made in the efficiency of perovskite-based devices, the stability of such materials remains a challenge. In this research paper, the role of substrate materials on which thin films of perovskites were deposited was examined, highlighting their critical importance for atmosphere-induced degradation. Indeed, CsPbBr$_3$ thin films sputtered on glass (soda lime and quartz) and indium tin oxide (ITO) resulted more stable, while those deposited on polycrystalline gold-coated glass were much more prone to degradation in a temperature- and moisture-controlled (43% relative humidity (RH)) atmosphere.

1. Introduction

Perovskites are a large family of chemically variable compounds structurally related to the mineral perovskite CaTiO$_3$. The ideal ABX$_3$ structure can be described as consisting of a corner-sharing [BX$_6$] octahedral with the A cation occupying the 12-fold coordination site formed in the middle of the cube of eight such octahedrons. The interest in compounds belonging to this family of crystalline structures is due to the surprisingly large number of elements that can occupy the A, B, and X sites, which result in a very wide and largely tunable range of physical properties.

Despite the fact that perovskite family members have been well known for more than a century [1], the recent synthesis of lead hybrid organic–inorganic perovskites improved their usefulness [2]. Constituting an organic cation in A, an inorganic cation, commonly Pb^{2+}, in B, and a halide in X (e.g., CH$_3$NH$_3$PbBr$_3$), hybrid perovskites have been proposed as innovative materials for many applications [3–5], especially related to solar energy conversion and the fabrication of diodes, lasers, light-emitting diodes (LEDs), and many others [5–7]. Their good capability of adsorbing light, long diffusion length of charge carriers, and tunable band gap, among others, are their main advantages with respect to traditional materials. In spite of their high efficiency, there are some drawbacks, the most important of which is the lack of chemical and structural stability [8–10]. The as-formed lead halide perovskites are subject to rapid degradation if exposed to moisture [11], ultraviolet (UV) irradiation [9,10,12] or heat [13,14]. This is mainly related to the hydration of organic cations, which leads to the formation of volatile compounds [15,16]. To overcome this issue, fully inorganic lead halide perovskites have been synthetized by replacing organic cations with inorganic ones [17]. This new class of perovskites showed slightly worse optical properties compared to hybrid ones, but boasted a larger operational stability, which is essential for practical applications [18]. CsPbBr$_3$ is one of the most

studied and promising fully inorganic perovskites thanks to its easy synthesis and profitable direct bandgap (2.3 V) [19].

Generally speaking, $CsPbBr_3$ thin films, as well as other perovskites, are obtained via wet chemistry deposition by means of two different approaches: (a) (single step) both precursor salts are mixed together, in a stoichiometric ratio, in a common solvent, before allowing the solvent to evaporate, leaving behind the perovskite deposition, or (b) (two steps) the precursors are dissolved into different solvents, singularly deposited as thin films by spin coating, deep coating, or spray coating, and then thermally treated to form the perovskite [7,20]. Unfortunately, these processes generally produce incoherent films, composed of tiny separated single crystals. This decreases the system efficiency since large grain boundaries increase the recombination rate. Deposition via melting both precursor salts in a quartz tube has also been proposed, but this approach turned out to be not suitable for industrial applications [21].

Recently, our group proposed a new, easy, and fast process for the deposition of thin, uniform, and chemically homogeneous perovskite films using magnetron sputtering technology [22]. This vacuum-based technique does not require the use of solvents, and the thickness can be regulated by controlling the time and rate of sputtering, which can be monitored "in situ" by means of a microbalance. This allows depositing the film on virtually every type of solid substrate. However, the nature of the substrate on which the film is deposited is not totally indifferent. Its chemical nature, as well as its crystalline structure, does affect the perovskite's nucleation and growth mechanism, leading to chemically, optically, and morphologically different deposits.

The aim of this work was to compare the stability of $CsPbBr_3$ thin films deposited onto different substrates when exposed to a moisture- and temperature-controlled atmosphere. According to suggested future applications, the perovskite films were grown on substrates commonly used for solar cells or optical devices: soda-lime glass, quartz glass, (111)-single-oriented polycrystalline gold, and indium tin oxide (ITO). The evolution of the thin-film surface's chemical and mineralogical composition, as well as their optical properties, was evaluated and discussed as a function of exposure time to the aggressive environment.

2. Materials and Methods

2.1. Chemicals

Cesium bromide and lead bromide were purchased from Alfa Aesar and, after drying in a muffle furnace (100 °C), used without further purification. The sputtering target was prepared following a previously described procedure [22]. Briefly, the precursor powders were weighed and mixed, in an equal molar ratio, in a milling vial. After milling (Retsch model MM400, Haan, Germany), the target was realized by pressing the powder for 24 h at 160 °C in a hydraulic press and then stored in a desiccator at room temperature before the experiments.

2.2. Substrates

Four different substrates were selected among the more commonly used in optical device fabrication: ITO, soda-lime glass, silica glass, and single-oriented polycrystalline gold. Glass slides coated with indium tin oxide (ITO) were purchased from Sigma Aldrich. Soda-lime glass (20 mm × 40 mm) slides for microscopy and silica glass slides (50 mm × 50 mm) were purchased from UGQ Optics. Single-oriented polycrystalline gold substrates were obtained "in house" by depositing 100 nm of gold on soda-lime glass slides (20 mm × 40 mm) via magnetron sputtering. Before gold sputtering, the slides were coated with 10 nm thick tantalum film, which acts as an interlayer improving the adhesion of gold toward glass. After deposition, using a gas torch, the samples were heated to obtain a prevalent Au (111)-oriented surface as previously described [23,24]. All substrates were cleaned with acetone and dried under pressurized air just before their use.

Table 1 summarizes the types and characteristics of the chosen substrates.

Table 1. Types of substrates used in this research. ITO, indium tin oxide; UV–Vis, ultraviolet–visible light; PV, photovoltaic.

Substrate Type	Chemical Nature	Mineralogical Properties	Optical	Conductive	Uses in PV and Optical Devices
Silica glass	SiO$_2$	Amorphous	Transparent UV–Vis spectrum	No	Optical windows and general use
ITO	In and Sn oxides	Crystalline	Transparent Vis spectrum	Yes	Transparent conductive substrate
Soda-lime glass	Commercial grade glass	Amorphous	Transparent Vis spectrum	No	General use
Gold	Metallic Au	Polycrystalline (111)-single-oriented	Reflective	Yes	Metallic back contact

2.3. Methods

Perovskite films were sputtered using a Korvus HEX system (Korvus Technology Ltd., Newington, UK) employing an argon plasma at rate of 0.05 nm/s up to 200 nm thick deposits, monitored using a quartz cell microbalance. To guarantee a homogeneous deposition rate and thickness, the substrates were fixed on a rotating sample holder set to 20 rpm during the deposition process. All substrates were located on the sample holder, obtaining the deposition of the films on the same run while equalizing the deposition parameters for all the samples. After the deposition step, each sample was divided into four pieces, one of which was used as a zero reference ("as prepared" sample), while the others were exposed to an aggressive environment.

The stability tests were carried out in a home-built climatic chamber in which temperature was maintained at 50 ± 1 °C with the relative humidity (RH) set to 43% using a saturated K$_2$CO$_3$ aqueous solution [25]. The nature of the crystalline phases constituting the samples was determined by X-ray diffraction (XRD) analysis performed by means of a model D8 Bruker diffractometer working in Bragg–Brentano mode. The optical properties were monitored using an ultraviolet–visible light (UV–Vis) Jasco V-670 double beam spectrometer equipped with an integration sphere, while the surface chemical composition was determined via X-ray photoelectron spectroscopy (XPS) constituting a VSW Scientific Instrument Limited model TA10 (Manchester, UK) equipped with a nonmonochromatic X-ray source and a VSW Scientific Instrument Limited model HA100 (Manchester, UK) hemispherical analyzer with a 16-channel detector. The spectra were collected in constant pass energy mode (22 eV) and the peaks were analyzed using CasaXPS software after Shirley-type background subtraction.

3. Results and Discussion

3.1. Structural Characterization

As mentioned above, the magnetron sputtering sample holder was large enough to allocate all four substrates tested. In such a way, all perovskite films were deposited exactly in the same conditions. Nevertheless, the XRD patterns collected on the "as-deposited" samples differed, demonstrating the active role of the substrate. Figure 1 displays the XRD pattern recorded on freshly prepared thin films. It is worth noting that, in accordance with previous reports [22] on glass substrates (soda lime and silica), the thin films were characterized by the presence of a nearly pure, even if strongly textured, CsPbBr$_3$ phase. Strong texturing was highlighted by the disagreement between the intensity ratio of the experimentally observed peaks and the literature data. In magnetron-deposited thin films, the dominant orientations were (100) and (202) (Figure 1), while the plane (121) was almost neglectable, strongly differing from the typical powdery CsPbBr$_3$ pattern (COD 1533062). On the other hand, in the deposit growth on single-oriented polycrystalline gold, the CsPbBr$_3$ phase was a minor constituent, and other peaks, not attributable to the gold substrate, were detectable in the spectrum (Figure 1, blue line).
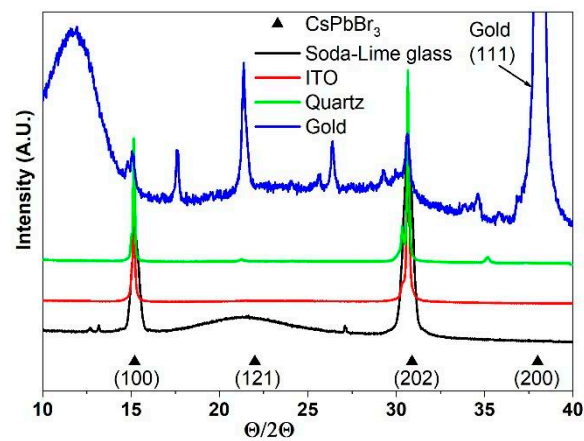
Figure 1. X-ray diffraction (XRD) patterns of the "as-deposited" thin films. Full triangles indicate the $CsPbBr_3$ phase diffraction peaks.

These differences were further highlighted during the ageing test. Figure 2 depicts the spectra of freshly prepared samples compared to those exposed to an aggressive environment (six days).
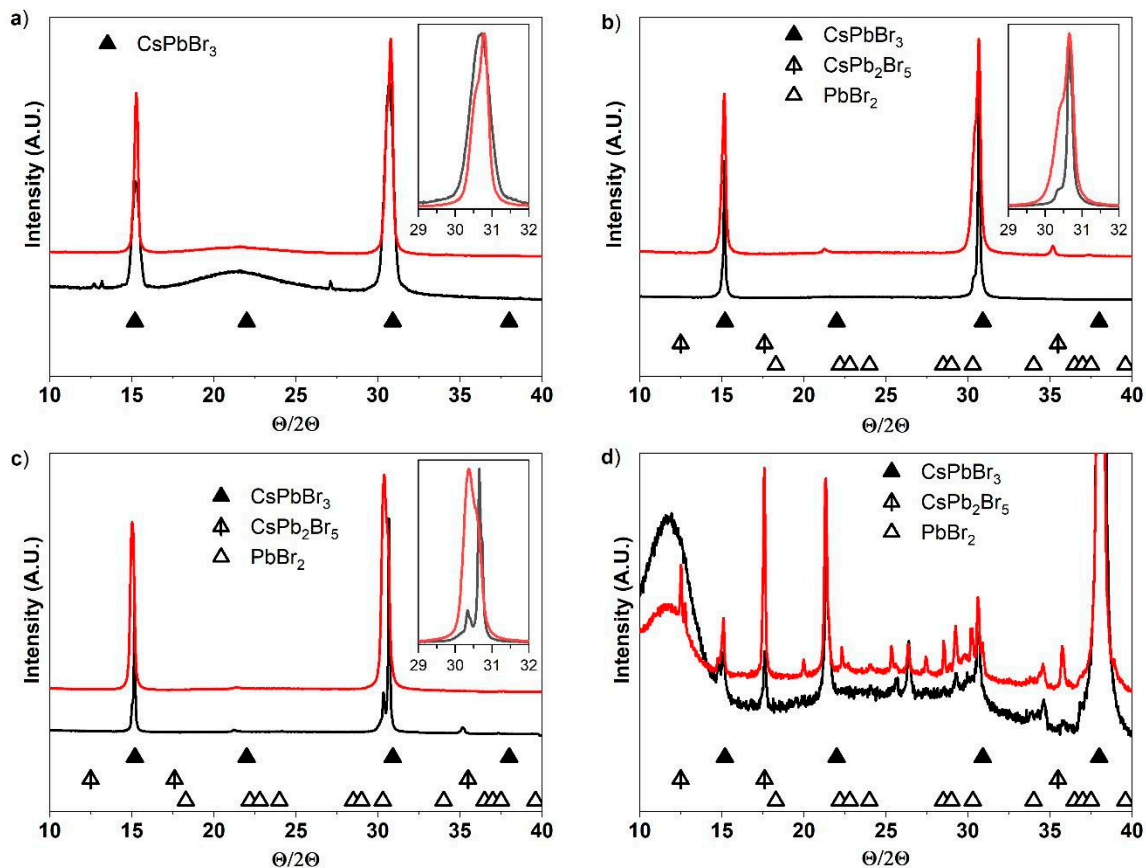

Figure 2. XRD patterns of the "as-prepared" (black lines) and aged (6 days, red lines) samples. As described in the legend, scatter symbols indicate the diffraction peaks for the most common byproduct phases: (**a**) quartz glass; (**b**) ITO; (**c**) soda-lime glass; (**d**) gold. Inset: zoom view of the region of the higher peak.

Even at the end of the aging test (6 days of exposure), in the samples grown on soda-lime glass, silica glass, and ITO, $CsPbBr_3$ still constituted the dominant mineralogical phase (Figure 2a–c), while the sample deposited on (111)-oriented gold presented a large number of peaks, some of which could be attributed to moisture-induced degradation byproducts such as $PbBr_2$ [11,26,27].

The insets of Figure 2a–c display a superimposed zoomed view of the most intense diffraction peaks ($CsPbBr_3$ (202)) of the "as-prepared" and aged samples. The "as-prepared" film obtained on silica glass (inset Figure 2a) presented a symmetric and well-defined, even if broad, diffraction peak. After the aging process, the peak appeared with two narrow components. This phenomenon can be reasonably explained considering that, during the aging process, the temperature and moisture cause the degradation of the perovskite and the consequent formation of a second peak. Moreover, the growth of the crystallites caused sharpening of the peaks. From the insets in Figure 2b,c, it is possible to note that, in the samples obtained on ITO and soda-lime glass, the peak at a lower angle was already present in the "as-prepared samples", meaning that these substrates promoted the immediate partial degradation of the perovskite film. The components forming the peak seemed to have a smaller width than the sample obtained on quartz glass, indicating bigger crystallites. After the aging process, the component attributed to the degraded perovskite increased.

3.2. Morphological Analysis

To verify the effect of the aging process on the sample morphologies, SEM images were acquired for the "as-prepared" (Figure 3) and aged samples (Figure 4).
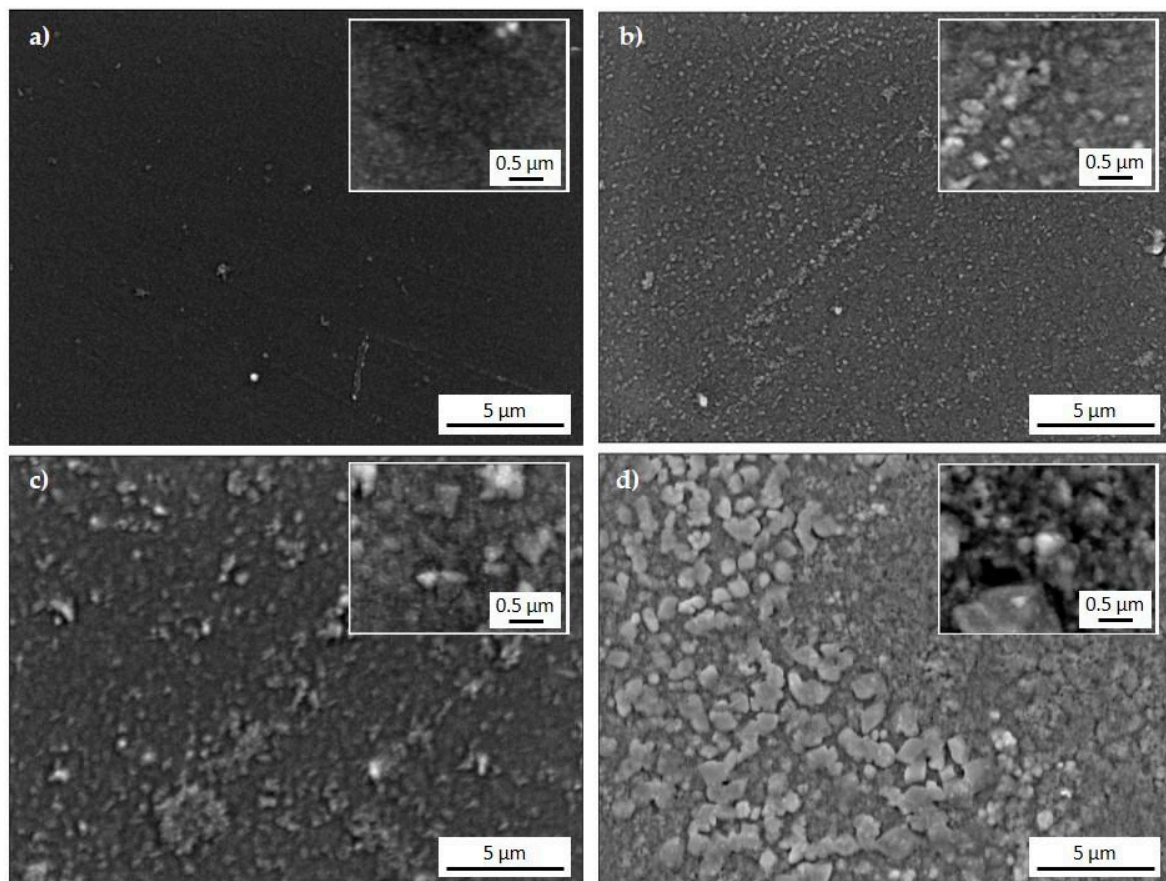

Figure 3. SEM images of the "as-prepared" samples: (**a**) quartz glass; (**b**) ITO; (**c**) soda-lime glass; (**d**) (111) gold. Insets display zoomed views of the same images.
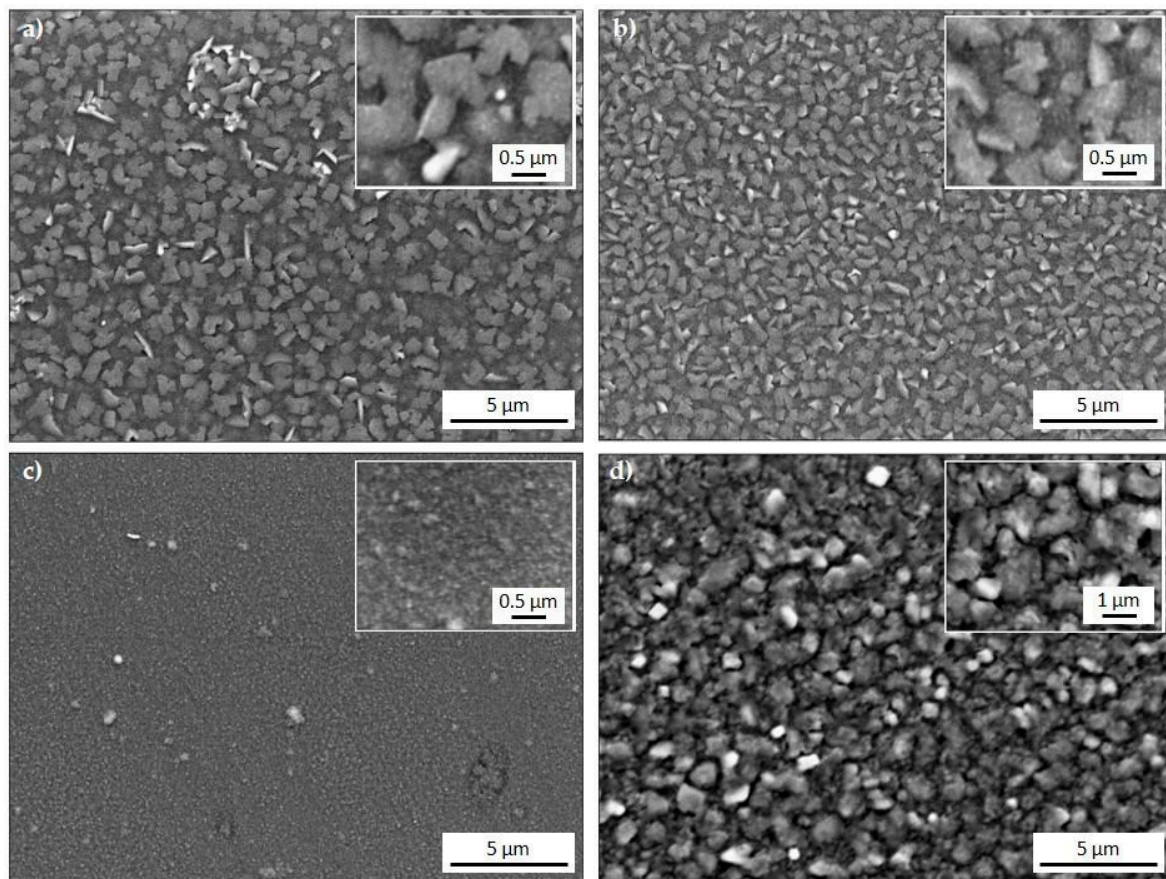
Figure 4. SEM images of the aged samples: (**a**) quartz glass; (**b**) ITO; (**c**) soda-lime glass; (**d**) gold. Insets display zoomed views of the same images.

It can be noted that, even though the deposition process was carried out in the same run and, therefore, the films were grown in exactly the same conditions, the obtained films displayed evident morphological differences. On quartz glass (Figure 3a), the deposit results constituted nanosized grains uniformly distributed all over the surface, seen at a high magnification level. A similar morphology, but with slightly larger granular features, was observed on ITO and soda-lime glass (Figure 3b,c), while, on (111)-gold, the film was unevenly distributed on the substrate (Figure 3d).

The morphology of the films after six days of aging is depicted in Figure 4.

On quartz glass and ITO, there was an evident recrystallization of the coating, promoting the formation of a large crystalline patchwork (Figure 4a,b). On soda-lime glass, there were apparently no significant morphological differences, while the film deposited on gold presented the most irregular morphology, constituting large barely interconnected granular structures which compromised the uniformity of the film (Figure 4d).

3.3. UV–Visible Light Absorption Spectra

The optical properties of the films were monitored as a function of degradation time by means of UV–Vis absorption measurements. Figure 5 depicts the normalized reflectance as a function of the wavelength for each sample. To normalize the data, the minimum value was subtracted from each reflectivity value, and the result was divided by the maximum, as reported in Equation (1).
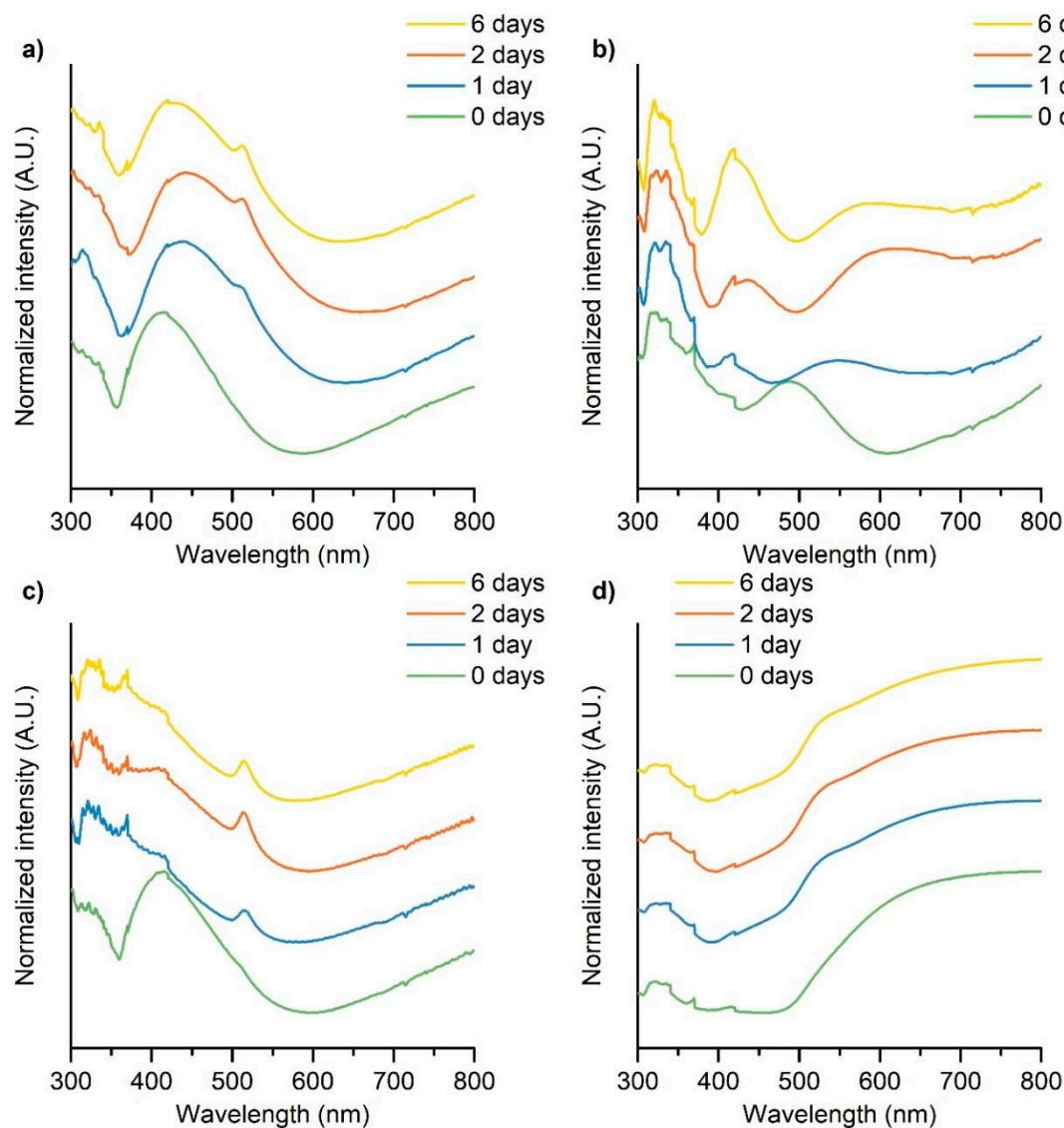
$$R_{norm.} = \frac{R_0 - R_{min}}{R_{max}}. \tag{1}$$

Figure 5. UV–Vis spectra in reflected light as a function of the time of exposure: (**a**) silica glass, (**b**) ITO, (**c**) soda-lime glass, and (**d**) gold.

The spectra collected on soda-lime and quartz glass closely resembled each other, whereas those collected on ITO and gold differed notably. It is also worth noting that the spectra recorded on pristine samples (green lines in Figure 5) did not present the peak at 520 nm, attributable to lead bromide, which is a typical byproduct of moisture degradation of lead bromide perovskites. However, this peak appeared in the spectra collected after just 1 day and became more and more intense as the aging test proceeded (Figure 5a,b).

The evidently different aspects of the spectra collected on gold-deposited samples can be attributed to the reflectivity of the substrate.

In the UV–Vis spectra, an edge of the reflectivity is typically visible, which allows calculating the bandgap value. However, in our case, this calculation was made difficult by the relatively modest thickness of the film.

3.4. Surface Chemical Evolution

Due to the small probing depth and the capability of chemically discerning different species of the same element, XPS was employed to monitor the chemical evolution of the surface of the samples as a function of the aging time. In particular, the lead XPS chemical shift provided very interesting clues

about the perovskite degradation process. Figure 6 depicts the XPS regions characteristic of the most intense and diagnostic XPS peak of lead (*6f* core transition), which was characterized by a doublet due to the spin-orbit coupling. Hereafter, we refer to the principal peak of the *f* transition as the right one. Lead peaks compatible with $CsPbBr_3$ were always present in the pristine samples (binding energy of the principal peak equal to 138.5 eV, doublet marked with red lines in the spectra reported in Figure 6). It is well known that the broadening of these peaks or the growth of secondary ones is related to the presence of lead in new chemical environments [12,28]. We observed this on the samples deposited on ITO, gold, and, to a minor extent, soda-lime glass (see Figure 6) upon the exposure to atmospheric moisture. On the other hand, on silica glass, the characteristic peak of lead remained almost identical throughout the stability test (Figure 6a). The presence of a peak at a lower binding energy with respect to $CsPbBr_3$ was reasonably attributable to the formation of reduced species such as Pb(0). It is also evident that the presence of these compounds was strictly related to the exposure to air, since it was never observed in the "as-prepared samples" and its intensity increased as a function of the exposure time. The XPS peaks of cesium and bromine did not present evident binding energy shifts and, therefore, did not provide useful information about the chemical evolution of the surface.
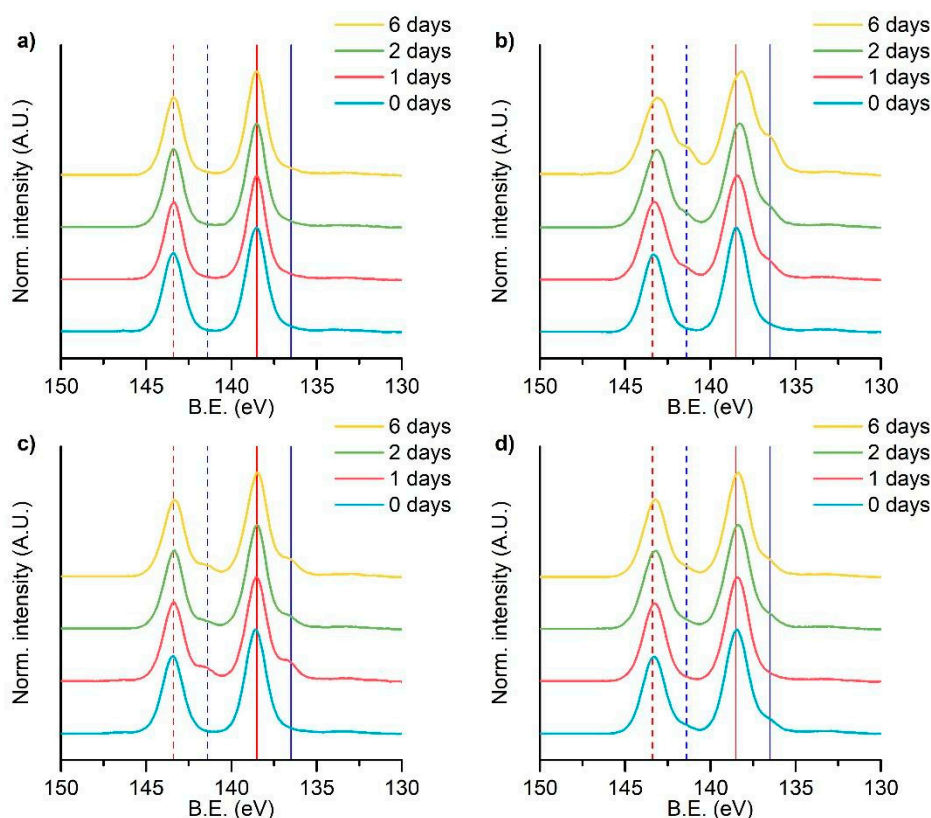

Figure 6. X-ray photoelectron spectroscopy (XPS) characteristic peaks of lead: (**a**) silica glass, (**b**) ITO, (**c**) soda-lime glass and (**d**) gold. Solid lines = main peaks; dashed lines = secondary peaks.

However, the relative intensity of XPS peaks is related to the atomic composition of the sample; therefore, it is possible to monitor the surface compositional trends as a consequence of the exposure time. Figure 7 displays the semi-quantitative elemental analysis for lead, cesium, and bromine as determined by XPS, employing tabulated sensitivity factors [28]. The expected composition of perovskite constitutes lead and cesium (20 at.%; one in every five atoms) and bromine (60 at.%; three in every five atoms). For the sake of clarity, in Figure 7, two red dashed lines are added: one at 20%, related to the expected amount of cesium and lead, and the other at 60%, related to the expected amount of bromine. As already observed, soda-lime and quartz glass presented the most stable and similar compositional profiles, while the surface of the perovskite thin films deposited on the other

two substrates was characterized by much more variable compositional trends indicating, on the whole, a less stable behavior in air. The surface of the film deposited on silica and soda-lime glass resulted enriched in Cs and depleted in Pb and Br, especially after the degradation tests. These data, together with XRD and UV–Vis results, suggest that the degradation of these samples caused a migration of lead bromide close to the surface of the film, bringing about a sort of passivation of the films that reduced their further degradation. On the other hand, samples obtained on gold and ITO substrates resulted enriched in cesium and lead and depleted in bromine, probably as a consequence of the quick degradation of the perovskite structure and the formation of volatile bromine byproducts that, in the ultra-high vacuum conditions in which XPS experiments were carried out, tended to be removed from the surface, indicating, on the whole, higher instability of the deposits grown on these substrates.
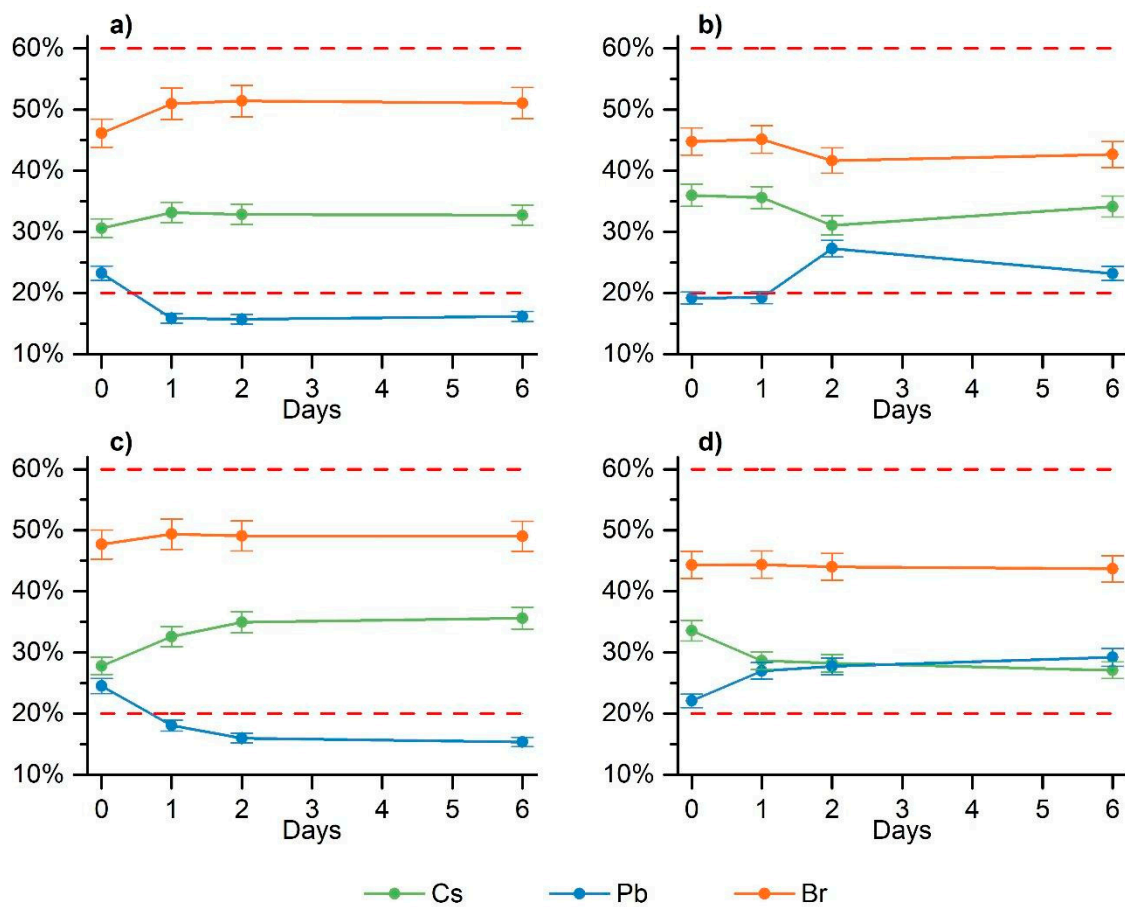

Figure 7. Compositional trends of the perovskite component as a function of exposure time for different substrates: (**a**) silica glass, (**b**) ITO, (**c**) soda-lime glass, and (**d**) gold. The red dashed lines at 20% and 60% represent the theoretical amounts of cesium and lead and of bromine, respectively, in $CsPbBr_3$.

4. Conclusions

This study proved that the stability of $CsPbBr_3$ in air is a crucial point for the industrial development of perovskite thin-film-based devices. Surprisingly, the sensitivity of $CsPbBr_3$ toward these environmental agents was not only amenable to structural defects, crystallite size, and crystalline orientation as previously reported, but also the nature of the substrate on which the perovskites were grown, which affected their stability and endurance. The thin films grown on amorphous (glasses) substrates and ITO displayed better performances, whereas the films deposited onto oriented gold resulted much more moisture-sensitive. The results of this preliminary investigation state the role of the substrate, as well as indicate a possible way of designing more stable and long-performing devices.

References

1. Rao, C.N.R. Perovskites. In *Encyclopedia of Physical Science and Technology*, 3rd ed.; Meyers, R.A., Ed.; Academic Press: Cambridge, MA, USA, 2001; pp. 707–714.

2. Green, M.A.; Ho-Baillie, A. Perovskite solar cells: The birth of a new era in photovoltaics. *ACS Energy Lett.* **2017**, *2*, 822–830. [CrossRef]

3. Huang, J.; Yuan, Y.; Thompson, B.C. *World Scientific Handbook of Organic Optoelectronic Devices: Volume 1: Perovskite Electronics*; World Scientific Publishing: Hackensack, NJ, USA, 2018; ISBN 9789813239845.

4. Stranks, S.D.; Snaith, H.J. Metal-halide perovskites for photovoltaic and light-emitting devices. *Nat. Nanotechnol.* **2015**, *10*, 391–402. [CrossRef] [PubMed]

5. Wu, J.R.; Thakur, D.; Chiang, S.E.; Chandel, A.; Wang, J.S.; Chiu, K.C.; Chang, S.H. The Way to Pursue Truly High-Performance Perovskite Solar Cells. *Nanomaterials* **2019**, *9*, 1269. [CrossRef] [PubMed]

6. Kanemitsu, Y.; Handa, T. Photophysics of metal halide perovskites: From materials to devices. *Jpn. J. Appl. Phys.* **2018**, *57*, 90101. [CrossRef]

7. Chen, Y.; Zhang, L.; Zhang, Y.; Gaoa, H.; Yan, H. Large-area perovskite solar cells–a review of recent progress and issues. *RSC Adv.* **2018**, *8*, 10489. [CrossRef]

8. Wang, D.; Wright, M.; Elumalai, N.K.; Uddin, A. Stability of perovskite solar cells. *Sol. Energy Mater. Sol. Cells* **2016**, *147*, 255–275. [CrossRef]

9. Shirayama, M.; Kato, M.; Miyadera, T.; Sugita, T.; Fujiseki, T.; Hara, S.; Kadowaki, H.; Murata, D.; Chikamatsu, M.; Fujiwara, H. Optical Transitions in Hybrid Perovskite Solar Cells: Ellipsometry, Density Functional Theory, and Quantum Efficiency Analyses for $CH_3NH_3PbI_3$. *Phys. Rev. Appl.* **2016**, *5*, 14012. [CrossRef]

10. Wang, F.; Ma, J.; Xie, F.; Li, L.; Chen, J.; Fan, J.; Zhao, N. Organic Cation-Dependent Degradation Mechanism of Organotin Halide Perovskites. *Adv. Funct. Mater.* **2016**, *26*, 3417–3423. [CrossRef]

11. Calisi, N.; Caporali, S.; Milanesi, A.; Innocenti, M.; Salvietti, E.; Bardi, U. Composition-Dependent Degradation of Hybrid and Inorganic Lead Perovskites in Ambient Conditions. *Top. Catal.* **2018**, *61*, 1201–1208. [CrossRef]

12. Lanzetta, L.; Aristidou, N.; Haque, S.A. Stability of Lead and Tin Halide Perovskites: The Link between Defects and Degradation. *J. Phys. Chem. Lett.* **2020**, *11*, 574–585. [CrossRef]

13. Akbulatov, A.F.; Frolova, L.A.; Dremova, N.N.; Zhidkov, I.; Martynenko, V.M.; Tsarev, S.A.; Luchkin, S.Y.; Kurmaev, E.Z.; Aldoshin, S.M.; Stevenson, K.J. Light or Heat: What Is Killing Lead Halide Perovskites under Solar Cell Operation Conditions? *J. Phys. Chem. Lett.* **2020**, *11*, 333–339. [CrossRef]

14. Ava, T.T.; Mamun, A.A.; Marsillac, S.; Namkoong, G. A review: Thermal stability of methylammonium lead halide based perovskite solar cells. *Appl. Sci.* **2019**, *9*, 188. [CrossRef]

15. Zhang, C.X.; Shen, T.; Guo, D.; Tang, L.M.; Yang, K.; Deng, H.X. Reviewing and understanding the stability mechanism of halide perovskite solar cells. *InfoMat* **2020**, *2*, 1034–1056. [CrossRef]

16. Kim, B.; Seok, S.I. Molecular aspects of organic cations affecting the humidity stability of perovskites. *Energy Environ. Sci.* **2020**, *13*, 805–820. [CrossRef]

17. Li, Z.; Song, C.; Rao, L.; Lu, H.; Yan, C.; Cao, K.; Ding, X.; Yu, B.; Tang, Y. Synthesis of Highly Photoluminescent All-Inorganic CsPbX3 Nanocrystals via Interfacial Anion Exchange Reactions. *Nanomaterials* **2019**, *9*, 1296. [CrossRef]

18. Kulbak, M.; Gupta, S.; Kedem, N.; Levine, I.; Bendikov, T.; Hodes, G.; Cahen, D. Cesium enhances long-term stability of lead bromide perovskite-based solar cells. *J. Phys. Chem. Lett.* **2016**, *7*, 167–172. [CrossRef]

19. Kulbak, M.; Cahen, D.; Hodes, G. How Important Is the Organic Part of Lead Halide Perovskite Photovoltaic Cells? Efficient CsPbBr3 Cells. *J. Phys. Chem. Lett.* **2015**, *6*, 2452–2456. [CrossRef]

20. Zhang, J.; Hodes, G.; Jin, Z.; Liu, S.F. All-Inorganic CsPbX3 Perovskite Solar Cells: Progress and Prospects. *Angew. Chem. Int. Ed.* **2019**, *58*, 15596–15618. [CrossRef]

21. Stoumpos, C.C.; Malliakas, C.D.; Peters, J.A.; Liu, Z.; Sebastian, M.; Im, J.; Chasapis, T.C.; Wibowo, A.C.; Young Chung, D.; Freeman, A.J.; et al. Crystal Growth of the Perovskite Semiconductor CsPbBr3: A New Material for High-Energy Radiation Detection. *Cryst. Growth Des.* **2013**, *13*, 2722–2727. [CrossRef]

22. Borri, C.; Calisi, N.; Galvanetto, E.; Falsini, N.; Biccari, F.; Vinattieri, A.; Cucinotta, G.; Caporali, S. First proof-of-principle of inorganic lead halide perovskites deposition by magnetron-sputtering. *Nanomaterials* **2020**, *10*, 60. [CrossRef]

23. Syed, M.; Glaser, C.; Hynes, C.; Syed, M. Thermal Annealing of Gold Thin Films on the Structure and Surface Morphology Using RF Magnetron Sputtering. *J. Mater. Sci. Eng. B* **2018**, *8*, 66–76.

24. White, J.R. Annealing behaviour of thin evaporated gold films. *Thin Solid Films* **1974**, *22*, 23–35. [CrossRef]

25. Greenspan, L. Humidity fixed points of binary saturated aqueous solutions. *J. Res. Nat. Bur. Stand. A Phys. Chem.* **1977**, *81*, 89–96. [CrossRef]

26. Dhaminiya, B.P.; Chhillar, P.; Roose, B.; Dutta, V.; Pathak, S.K. Unraveling the effect of crystal structure on degradation of methylammonium lead halide perovskite. *ACS Appl. Mater. Interfaces* **2019**, *11*, 22228–22239. [CrossRef]

27. Di Girolamo, D.; Ibrahim Dar, M.; Dini, D.; Gontrani, L.; Caminiti, R.; Mattoni, A.; Graetzel, M.; Meloni, S. Dual Effect of Humidity on Cesium Lead Bromide: Enhancement and Degradation of Perovskite Films. *J. Mater. Chem. A* **2019**, *7*, 12292–12302. [CrossRef]

28. Moulder, J.F.; Stickle, W.F.; Sobol, P.E.; Bomben, K.D. *Handbook of X-ray Photoelectron Spectroscopy*; Chastain, J., Ed.; Perkin-Elmer Corp.: Eden Prairie, MN, USA, 1992.